Molecular catalytic system for efficient water splitting

Joya, K.S.

Chapter 2

Electrochemical Methods for Studying Catalytic Water Splitting: A Ru-red Model Study

ABSTRACT

To study the possibility of water oxidation by Ru-red, $[(NH_3)_5Ru\text{-}O\text{-}Ru(NH_3)_4\text{-}O\text{-}Ru(NH_3)_5]Cl_6$, and ruthenium oxide in acidic media, oxygen evolution measurements are performed with the electrochemical rotating ring-disk electrode (RRDE) and on-line electrochemical mass spectrometry (OLEMS), and are complemented by spectro-electrochemical investigations during water splitting catalysis with *in situ* surface enhanced Raman spectroscopy (SERS). Ru-red dispersed in acid electrolyte and immobilized on a gold surface without Ru-red in solution has been subjected to anodic water oxidation experiments. The catalytic behaviour of electrodeposited ruthenium oxide thin film on the Au disk was also studied for oxygen generation and the results were compared with Ru-red. On a gold electrode in sulphuric acid solution containing Ru-red, we observe one electron oxidative conversion to a higher oxidation state ruthenium compound, Ru-brown $[(NH_3)_5RuORu(NH_3)_4ORu(NH_3)_5]^{7+}$ at *ca.* 0.74 V (vs. NHE), which was supported by *in situ* SERS experiments. RRDE analyses produce oxygen detection signals at the ring around 1.25 V (vs. NHE). However, the oxygen formation is not validated by the OLEMS analysis. In contrast, a Ru-red functionalized gold electrode in same electrolyte solution without having Ru-red gives rise to the water oxidation signal and the oxygen onset potential is just above 1.45 V (vs. NHE). Oxygen reduction signals are present on the RRDE current-potential profile, which were confirmed for oxygen evolution by real time oxygen detection in OLEMS set up. The data provide evidence for water oxidation close to the equilibrium potential of 1.23 V (vs. NHE) in sulphuric acid by an immobilized ruthenium based molecular catalyst.

Based on: K.S. Joya, H.J.M. de Groot and M.T.M. Koper (*to be submitted*)

2.1. INTRODUCTION

The introduction of renewable energy [1] carriers based on solar energy and using water as a raw material is stimulated by the worries for global warming and decreased availability of oil and gas [2-6]. Efficient water oxidation is challenging from a catalytic standpoint, and the most critical hurdle is to design and make a stable multi-electron transfer catalyst that can split water at high turnover rates [7]. The Mn_4O_4Ca cluster in natural photosystem-II is an inspiring model of an oxygen evolving complex that catalyzes four electron water oxidation with a moderate activation energy and electrochemical overpotential [8-13]. This has fueled scientific interests towards the construction of artificial water splitting catalytic systems that attempt to mimic closely the natural catalyst in terms of configuration and efficiency [14-21]. Various ruthenium and manganese complexes as discussed in the previous chapter have been considered as "artificial" water splitting catalysts, and a maximum turnover number up to 1500 is obtained [21-26]. Generally, these systems are investigated by using chemical oxidants to promote four electron water oxidation [27].

Ru-red, a di-μ-oxo-bridged trinuclear ruthenium amine complex $[(NH_3)_5RuORu(NH_3)_4ORu(NH_3)_5]Cl_6$ (Fig. 2.1) has been shown to be catalytically active for water splitting [28]. While this system has also been studied in an electrochemical environment, the mechanism of electrocatalytic oxygen evolution on Ru-red was not studied in much detail [28-34]. On a basal plane pyrolitic graphite electrode (PGE) in 0.1 M H_2SO_4 aqueous solution, Ru-red was found to undergo one electron conversion into Ru-brown and ultimately to water oxidation and dioxygen formation, which was detected by gas chromatography combined with mass spectrometry (GC-MS) [28,32]. In acidic and aqueous solutions at room temperature, the oxo-bridges are not stable, which facilitates thermal and photo-induced decomposition of Ru-red into monomeric ruthenium compounds [28,34]. On the other hand, Ru-brown was reported to be unaffected by thermal or photochemical decomposition in 0.05 M nitric acid [35].

Combined spectral and electrochemical studies of a solution containing Ru-red did not reveal any decomposition of the complex during the electrochemical process [32,34]. It has also been reported that the anodic oxidation of Ru-red led to the formation of ruthenium-brown without the formation of RuO_2 [28]. In addition, there is only scant direct evidence that Ru-red did not convert into RuO_2 before or during water splitting. This issue is especially relevant as RuO_2 is an extremely potent catalyst for oxygen evolution [36]. *In situ* visible absorption spectroscopy experiments by Ramaraj and Kaneko showed that Ru-brown is unstable when conditions for homogeneous water oxidation are applied, while incorporation in a heterogenous Nafion membrane stabilizes the complex against decomposition and exhibits catalytic activity [32,37].

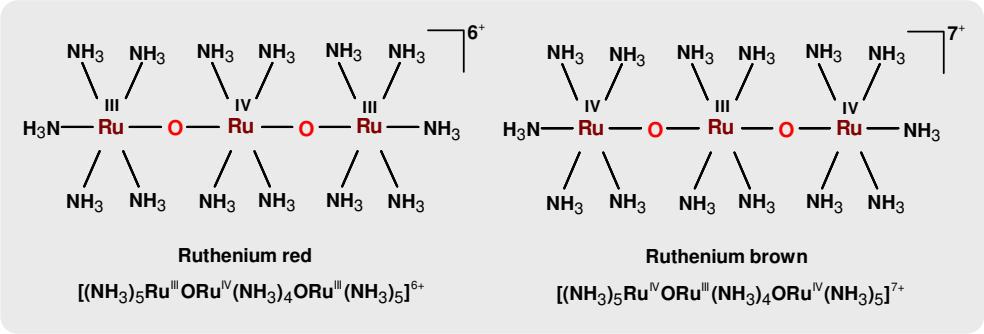

Figure 2.1. Chemical structural formula of (**left**) Ru-red and (**right**) Ru-brown showing ruthenium and oxygen architecture and metal oxidation states. Three Ru nuclei are connected by two oxo-bridges in amine ligands surrounding.

This chapter follows up on the observation by Kaneko *et al*. [30] that Ru-red immobilized on gold and platinum [38,39] electrodes is also active for electrocatalytic water oxidation. As Ru-red on polycrystalline gold disk (Au_{disk}) is one of the simplest examples of a surface modified with a molecular catalyst for water oxidation, it is of interest to study the electrochemical and spectroelectrochemical characteristics of this system. In addition, the Ru-red/Au_{disk} system enables the application of two established (spectro-)electrochemical techniques for its further characterization that will be used in this chapter.

First of all, application of the RRDE technique allows for the *in situ* detection of oxygen generated at the Ru-red/Au_{disk} electrode by a platinum ring (Pt_{ring}) biased for oxygen reduction. The RRDE technique, which has been used for the study of oxygen evolution by oxidic catalysts and oxygen reduction [40-43], has been applied very rarely in electrochemical studies of molecular catalysts for water oxidation. Second, using gold as a substrate for Ru-red permits the application of SERS to probe the vibrational signatures of the catalyst system at the metal-electrolyte interface. Using these two techniques, water oxidation catalyzed by Ru-red was investigated for a bare Au_{disk} electrode in contact with a sulphuric acid electrolyte solution containing Ru-red, and for a Ru-red functionalized gold electrode, without Ru-red in the electrolyte solution. In parallel, we compare the properties of Ru-red on gold with those of another well known Ru-based water oxidation catalyst, ruthenium oxide (RuO_x), by using the same experimental conditions as for Ru-red. The main objectives of this work are thus to apply the RRDE for sensitive and direct oxygen measurements, and validating its data using an OLEMS set up, along with the SERS investigation for interfacial vibrational characterization during water splitting catalysis by the molecular complexes, and comparing the activities of the Ru-red and the RuO_2 catalysts.

2.2. RESULTS AND DISCUSSION

2.2.1. RRDE Studies

Figure 2.2 summarizes the results obtained with the RRDE setup for three different experiments: oxygen evolution on a bare gold disk electrode (dash-dotted line), water oxidation on a clean Au electrode with Ru-red in solution (solid line), and oxygen evolution on an Au electrode functionalized with Ru-red (dashed line) in deoxygenated and Ar-saturated 0.1 M H_2SO_4 aqueous solution as explained in the section 2.4 of this chapter. Figure 2.2a shows the disk current density (J_D), while the lower panel displays the corresponding ring current density (J_R). Both J_D and J_R are obtained simultaneously at a rotation rate of 700 rpm by cycling the potential of

the Au_{disk} between 0.50 and 2.10 V (vs. NHE) at a scan rate of 20 mVs^{-1}, while the Pt_{ring} was kept at 0.44 V (vs. NHE). For this ring potential, the oxygen reduction on the polycrystalline Pt_{ring} is limited by mass transport [44,45]. Figure A2.1 (Appendix A2) shows voltammetric scans at the platinum ring for different gold disk potentials for the validation of oxygen evolution during the oxidation process at high disk potentials.

It is evident from Figure 2.2a that on a bare Au electrode, oxygen evolution starts just above 1.80 V, which is in good agreement with the results reported by Vergé *et al.* [43]. The corresponding reduction current at the ring is indeed due to the oxygen reduction provided that no oxidation products are coming from the gold disk that can be reduced or detected at the ring under given conditions (Fig. 2.2b). The collection efficiency ($N=-I_{Ring}/I_{Disk}$) is lower than the theoretical value, *i.e.* $N_{exp} \approx 0.025$ vs. $N_{theo} = 0.256$ (see Materials and Methods section). The deviation corroborates observations made by Vergé *et al.* using a gold ring as well as by various other authors employing the RRDE technique to investigate the oxygen evolution reaction [Ref. 43 and references therein]. The low collection efficiency is attributed to the formation of oxygen bubbles at the anode catalyst, which is difficult to assess during the potential scanning on a disk electrode in the RRDE system.

The formation of gold oxides and oxygen evolution occur simultaneously at higher potential of the Au_{disk} electrode. Hence, the measured anodic current for oxygen evolution at the Au electrode is the sum of the gold oxide growth current and the water oxidation current, which dominates at higher potential [43]. Although the difference between the experimental and theoretical values prevents a quantitative analysis of the results, the RRDE provides unequivocal detection of oxygen formed by the catalytic water oxidation on the disk electrode. RRDE analyses reveal that both Ru-red systems (*i.e.* one with Ru-red in solution and one with Ru-red immobilized on the Au disk but not present in solution) exhibit a significantly lower overpotential for water oxidation than the bare gold electrode.

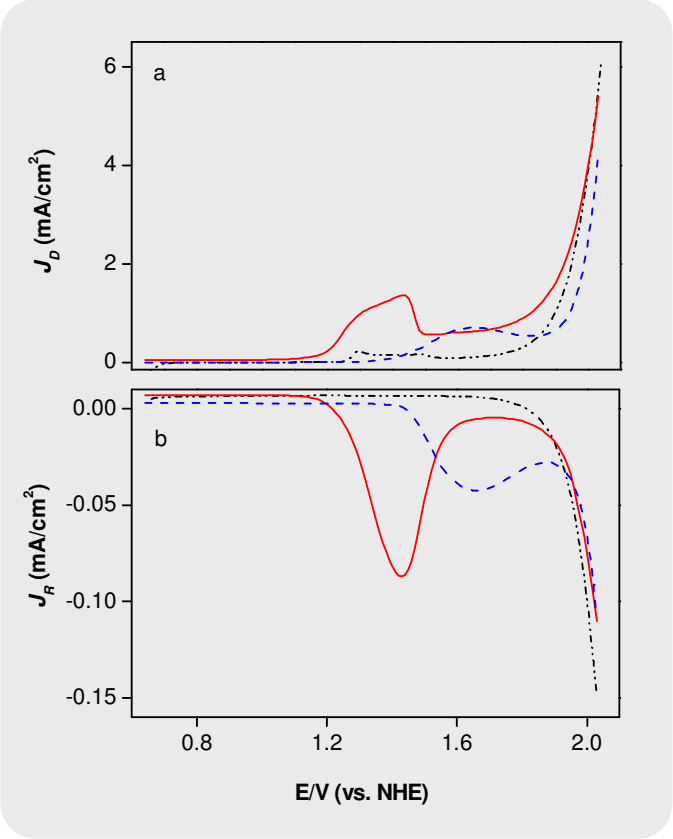

Figure 2.2. Forward potential scans for oxygen evolution current densities (J_D); (**a**) for the bare Au_{disk} (dash dotted line), the bare Au_{disk} in 0.1 M H_2SO_4 solution containing 0.035 mM Ru-red (solid line) and a gold disc functionalized with Ru-red (dashed line) in deoxygenated 0.1 M H_2SO_4 electrolyte solution, and (**b**) corresponding oxygen reduction current densities (J_R) on the Pt_{ring} for the RRDE assembly in 0.1 M H_2SO_4 aqueous solution. Rotation rates were 700 rpm, scan rates 20 mV/sec and the ring potential was 0.44 V (vs. NHE).

With Ru-red in solution, the onset of oxidation is at a potential as low as 1.23 V (vs. NHE), mirrored by oxygen reduction current at the Pt_{ring} (Fig. 2.2b) assuming that no adsorption or electrodeposition of the catalyst on the Pt_{ring} occurs and no simultaneous formation of the Ru-red oxidation products at the gold disk which may get in contact with the ring during rotation at 700 rpm. To show that the current measured at the ring is indeed due to oxygen coming from the disk, we have investigated the voltammetry at the ring while keeping the disk potential at ~1.35 V (Fig. A2.2). The oxygen reduction wave was not observed around 0.44 V,

at the Pt ring, but a current wave appeared at <0.15 V, when the disk potential kept at 1.23 V, which becomes more positive when the potential rises. This current might be associated with the oxygen detection at less positive potential on the Pt_{ring} that is in contact with the Ru-red in the electrolyte solution. This could block the ring surface for effective oxygen reduction.

On the other hand, the collection efficiency for this experiment, *ca*. 0.05, is less than the theoretical value. The low collection efficiency is in line with the formation of oxygen and oxygen bubbles at the disk electrode, and this renders a detailed quantitative interpretation of the RRDE results unfeasible. The oxygen evolution ability reaches a maximum at *ca*. 1.44 V and then drops, reflected by a similar decrease in reduction current on the ring. This loss in catalytic activity at higher potentials may be ascribed to over-oxidation of the Ru-based catalyst. Similar disk and ring voltammetry is observed in subsequent scans, although overall currents decrease with each scan, indicating a gradual loss of the catalytic performance of Ru-red for water oxidation. Variation of the catalyst concentration by four to five times did not have a significant effect on the catalytic activity of Ru-red, regardless of whether the catalyst was dissolved in 0.1 M H_2SO_4 or adsorbed on the Au_{disk}.

Interestingly, oxidation wave on the Ru-red functionalized Au electrode starts at *ca.* 1.44 V (vs. NHE), approximately 210 mV higher than the experiment with Ru-red in solution (Fig. 2.2). In this case, the current at the ring cannot be due to another process than oxygen reduction, as there is virtually no Ru-red in the solution. No colouring of the solution was observed due to free Ru-red during potential scanning of the RRDE at 700 rpm, indicating that there was no detachment of Ru-red from the Au_{disk} during cycling at this rotation rate. The experimental collection efficiency, *ca*. 0.05, is still lower than the theoretical value, but similar to the system with Ru-red in solution. Also this system exhibits a maximum in catalytic activity within one scan, and a decrease in catalytic activity with each subsequent voltammetric scan, pointing again to instability of the Ru-red catalyst at higher potential. Cycling the potential of the ring, while the potential of

the Au_{disk}, functionalized with Ru-red, was kept around 1.45 V, reveals a reduction current at the ring in the oxygen detection regime when the catalyst was not present in the solution (Fig. A2.3). The current increases with rising potential and this indicates the formation of oxygen at *ca*. 1.44 V for the Au functionalized Ru-red system.

Kaneko *et al*. has reported the electrochemistry of Ru-red in 0.1 M H_2SO_4 aqueous solution at a poly(styrene sulphonate)-coated basal plane pyrolitic graphite (BPG) electrode. They observed the conversion of Ru-red into Ru-brown (Eq. 2.1) and cyclic voltammogram exhibited redox features during the oxidative scan and proposed that the Ru^{V}-O-Ru^{V}-O-Ru^{V} (Ru^{V}-Ru^{V}-Ru^{V}) state releases oxygen [34]. The oxidative transitions take place at 1.08 V for Ru^{IV}-Ru^{IV}-Ru^{IV}/Ru^{IV}-Ru^{III}-Ru^{IV}, 1.19 V for to Ru^{IV}-Ru^{V}-Ru^{IV}/Ru^{IV}-Ru^{IV}-Ru^{IV}, 1.32 V for Ru^{V}-Ru^{IV}-Ru^{V}/Ru^{IV}-Ru^{V}-Ru^{IV} and 1.40 V for Ru^{V}-Ru^{V}-Ru^{V}/Ru^{V}-Ru^{IV}-Ru^{V} (vs. NHE). In our study on a gold electrode in 0.1 M H_2SO_4, we were unable to resolve these oxidation peaks for Ru-red conversion into Ru-brown and its higher oxidation states.

$$\underset{\text{(Ru-red)}}{Ru^{III}\text{-O-}Ru^{IV}\text{-O-}Ru^{III}} \underset{\text{Neutral/OH}^-,\ +e^-}{\overset{\text{Acid (H}^+\text{), -e}^-}{\rightleftharpoons}} \underset{\text{(Ru-brown)}}{Ru^{IV}\text{-O-}Ru^{III}\text{-O-}Ru^{IV}} \qquad (2.1)$$

In order to compare the activity of the Ru-red-Au system with RuO_2, a hydrous ruthenium oxide ($RuO_x \cdot nH_2O$) film was electrodeposited on a roughened Au_{disk} surface in the RRDE assembly. Oxygen evolution on the RuO_x-modified Au electrode starts close to 1.30 V and drops dramatically at *ca*. 1.45 V (Figure 2.3), nearly identical to the oxygen evolution characteristics of a solution containing Ru-red in contact with gold electrode (Fig. 2.2). This also implies the possibility of the oxidative decomposition of the Ru-red near 1.25 V at gold disk to form some oxide of ruthenium. *In situ* SERS analyses for Ru-red and electrodeposited ruthenium oxide are conducted for further elucidation (see section 2.2.3). The electrodeposited oxide of ruthenium on the gold surface leads to higher currents for

water oxidation compared to Ru-red, but this may be simply due to a higher number of active catalytic sites on the Au electrode.

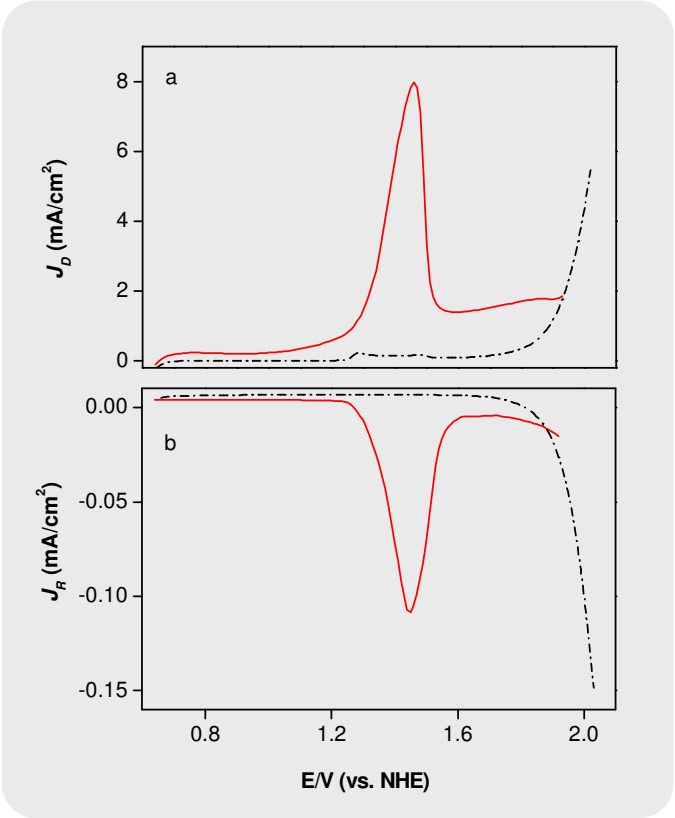

Figure 2.3. (**a**) Forward potential scans for oxygen evolution current densities (J_D) for the bare Au_{disk} electrode (dash dotted line) and for electrodeposited ruthenium oxide on Au_{disk} in deoxygenated Ar-saturated 0.1 M H_2SO_4 electrolyte solution (solid line), and (**b**) corresponding oxygen reduction current densities (J_R) on the Pt_{ring} in the RRDE assembly in 0.1 M H_2SO_4 aqueous solution. Rotation rates were 700 rpm, scan rates 20 mV/sec and the ring potential was 0.44 V (vs. NHE).

Similar to the systems shown in Figure 2.2, the experimental collection efficiency of the RRDE assembly consisting of a RuO_x-modified Au electrode and a Pt_{ring} is again significantly below the theoretical value suggesting oxygen bubble formation at the Au anode along with the possibility of higher metal oxide generation. Previous RRDE studies of oxygen evolution of Ru-oxide have shown that RRDE techniques may be used to detect both oxygen and Ru corrosion

products, such as RuO_4 but we did not attempt to detect the oxidation products [41,46].

Comparing the oxidation current on the gold disk with the reduction current on the platinum ring, it is observed that the oxidation current at the onset of the peak, between *ca*. 1.0 and 1.22 V (Fig. 2.3), is not due to oxygen evolution. This oxidation current must therefore be ascribed to the further oxidation of the Ru deposits. A similar observation was made by Wohlfahrt-Mehrens and Heitbaum, who followed the oxygen evolution by a ruthenium film electrode in sulphuric acid employing differential electrochemical mass spectrometry (DEMS) [47]. Their experiment shows an oxidation current between 1.1 and 1.4 V (vs. NHE) that is not accompanied by the detection of oxygen in the DEMS, whereas the high oxidation current for potentials higher than 1.4 V (vs. NHE) leads to a significant detection of oxygen in the online mass spectrometer. In a recent study, cyclic voltammetry of uncalcined and calcined (350–550° C) RuO_2 deposits in 1 M H_2SO_4 at 20 mV/sec has shown irreversible current peaks at *ca*. 0.70 V (vs. NHE). These current peaks have been assigned to the valence state change of the ruthenium in oxide matrices from Ru^{III} to Ru^{IV} [48]. However in this study, the current-potential profile of the electrodeposited RuO_x on Au is almost a smooth curve, without significant voltammetric features (Fig. 2.3a).

In another set of experiments, Ru-red immobilization and ruthenium oxide electrodeposition was performed on a basal plane graphite disk. The results for oxygen evolution are compared with those obtained on Au substrate. The oxygen onset occurs above 1.37 V (vs. NHE) on the BPG-RuO_x matrix as indicated by reduction currents at the ring. Interestingly, the BPG modified Ru-red electrode displays the oxygen evolution wave beyond 1.65 V (vs. NHE) reflected by the ring detection current (Fig. 2.4). No oxygen reduction currents were observed for the bare BPG up to the limiting potential of the experimental setup. Later, the oxygen generation was confirmed by employing a calibrated oxygen sensor connected with an oxy-meter [23]. The reason for different activity of Ru-red on

Au and graphite electrodes is not clear at present and further experiments need to be done to address this question.

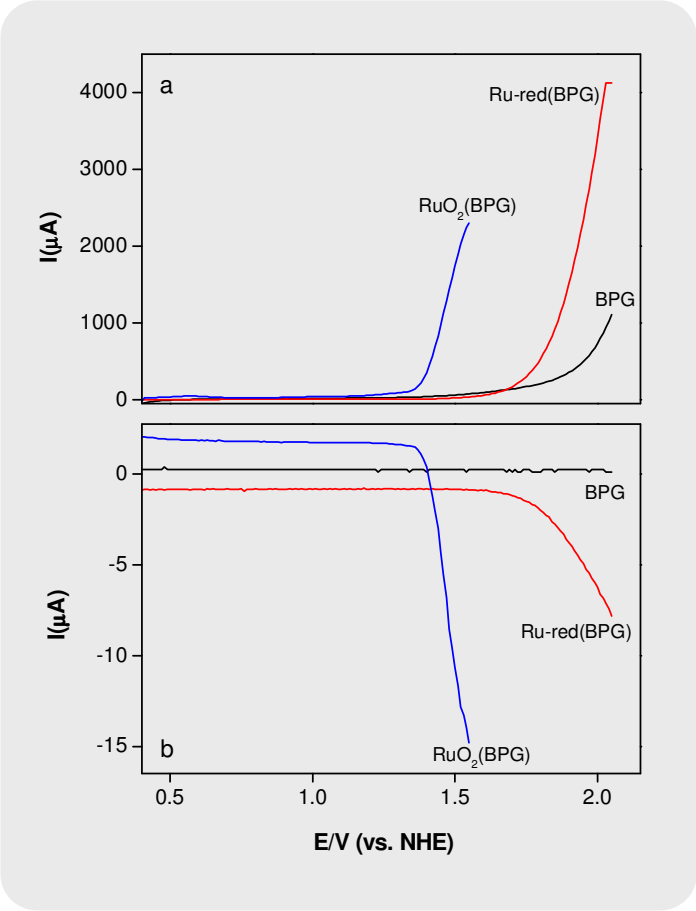

Figure 2.4. Forward potential scans for oxygen evolution currents: (**a**) for the bare BPG disk, the BPG functionalized with Ru-red and for electrodeposited RuO_x on BPG disk in deoxygenated 0.1 M H_2SO_4 electrolyte solution, and (**b**) corresponding oxygen reduction currents on the Pt_{ring} for the RRDE assembly in 0.1 M H_2SO_4 aqueous solution. Rotation rates were 700 rpm, scan rates 20 mV/sec and the ring potential was 0.44 V (vs. NHE).

2.2.2. OLEMS Analysis

Oxygen confirmation experiments on gold disk in contact with the tri ruthenium catalyst were conducted using online electrochemical mass spectrometry measurements in acidic medium. Real-time oxygen generation and detection

analyses were performed during linear sweep voltammetric scans, from the Au electrode immersed in the electrolyte solution containing Ru-red and the gold disk functionalized with the catalyst without Ru-red in the solution. The Au_{disk} functionalized with Ru-red and without Ru-red in the solution reveals oxygen detection by the OLEMS measurements between 1.50 and 1.60 V vs. NHE (Fig. 2.5a), thus verifying the RRDE studies (Fig. 2.2). No attempts were made to record the oxygen while scanning back from ~1.9 V in the same experiment.

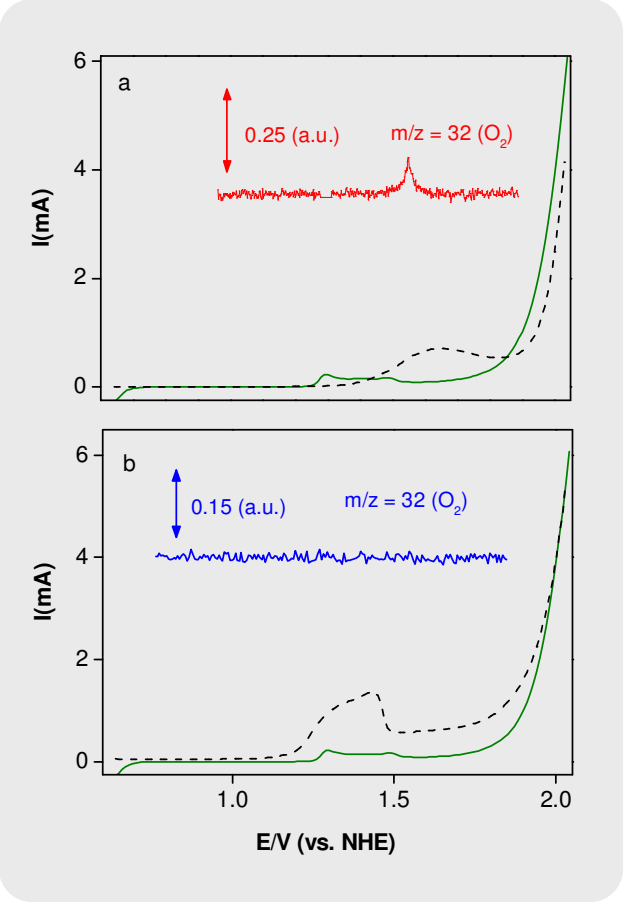

Figure 2.5. Forward potential voltammetry showing the oxygen evolution current and corresponding real time OLEMS measurements (red and blue curves) for (**a**) the gold disk functionalized with Ru-red in deoxygenated 0.1 M H_2SO_4 solution containing no Ru-red and (**b**) a bare gold disk in 0.1 M H_2SO_4 solution containing 0.035 mM Ru-red (1.0 mV/sec). The green solid lines in both panels are the CV's of the bare Au disk 0.1 M H_2SO_4 solution.

There is no evidence from the OLEMS analysis for the possible generation of peroxide intermediates during water oxidation and the final catalytic phase involved in the dioxygen evolution from Ru-red as detected by OLEMS [28,34]. The oxygen detection peak suddenly declines and flattens at a potential of ~1.63 V suggesting decomposition or/and instability of Re-red on the gold surface. This corroborates our inference from RRDE that the current regime above 1.71 V does not involve the formation of oxygen (Fig. 2.2). Surprisingly, no oxygen (m/z = 32) formation was detected between 1.23 – 1.65 V (vs. NHE) for the bare Au in contact with the solution containing Ru-red (Fig. 2.5b), which does not validate our inferences obtained from RRDE experiments (Fig. 2.2). A preliminary controlled-potential electrolysis experiment was performed for the gold disk functionalized with the catalyst without Ru-red in the solution, but the catalyst was found to be unstable for longer time exposure in the aqueous sulfuric acid.

2.2.3. Electrochemical SERS Investigations

In situ SERS experiments were conducted as described in section 2.4. Figure 2.6a shows the *in situ* SER spectra of Ru-red on gold at selected potentials when Ru-red was present in solution and Figure 2.6b shows the same spectra for Ru-red immobilized on gold (RRA) without Ru-red in solution. Various Raman shifts were observed for the trinuclear ruthenium-amine catalyst and peak assignments can be made by comparison with the data reported in the literature. Table 1.1 gives the Raman shifts (cm^{-1}) for Ru-red and Ru-brown in the 100-1000 cm^{-1} region, which is the finger print region of Ru-red and Ru-brown [49,50]. In the solid state Ru-red has a nearly linear backbone structure with octahedral surroundings of the metal ions and near C_{4v} symmetry due to packing effects on the molecular skeleton [51]. Raman data have indicated that Ru-red adopts a near D_{4h} symmetry in solution, with the octahedrons aligned along the backbone, albeit without perfect inversion symmetry, and that Ru-brown has a similar structure [50,52-54]. For the D_{4h} symmetry 6 modes are Raman active, which have been assigned in a series of investigations (Table 1.1) [50,54].

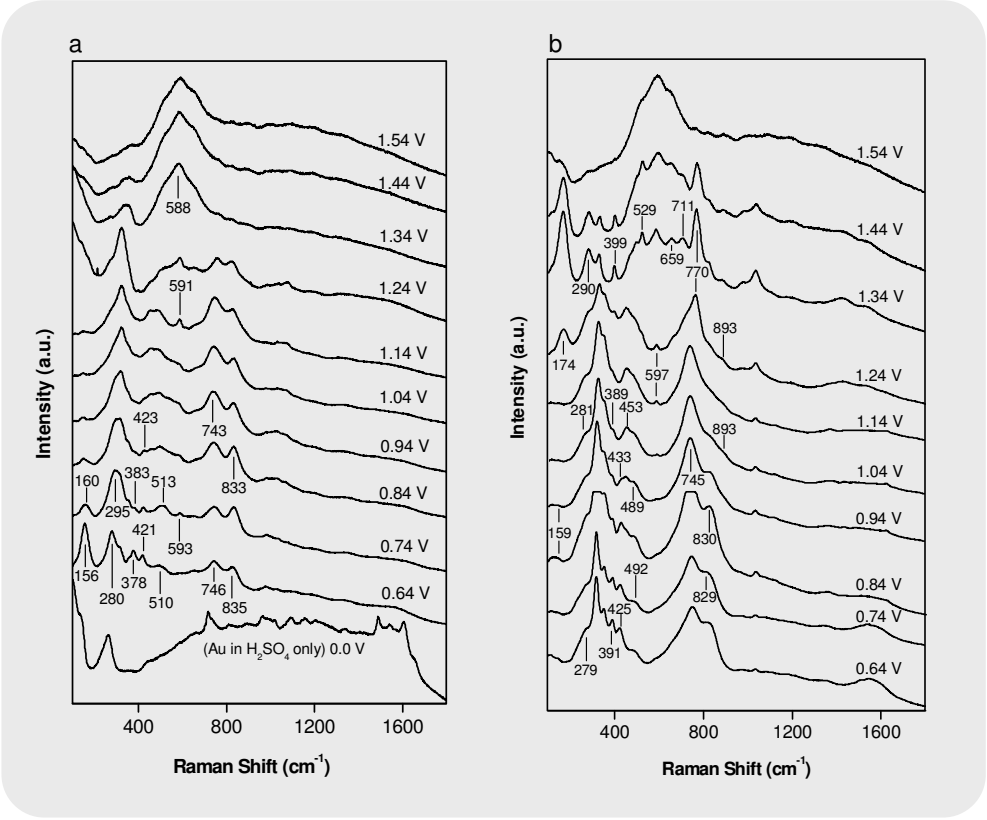

Figure 2.6. Selected potential-dependent *in situ* electrochemical SER spectra for (**a**) the freshly roughened Au_{disk} electrode in deoxygenated 0.1 M H_2SO_4 aqueous solution containing 0.035 mM Ru-red and (**b**) Ru-red functionalized freshly roughened Au_{disk} electrode in deoxygenated Ar-saturated 0.1 M H_2SO_4 aqueous solution. The starting potential was 0.6 V and it was increased to 1.5 V (vs. NHE) in successive 0.1 V increments.

The deviation from the D_{4h} is apparent from the observation of a strong antisymmetric mode at 825 nm in Ru-red. Although the principal Raman characteristics of Ru-red and Ru-brown are very similar, the ν_1, ν_5, ν_6, and ν_7 bands for Ru-brown are all shifted to higher frequency compared to the corresponding vibrations in Ru-red, by 34, 13, 21 and 15 cm^{-1}, respectively, indicating a stiffening of the backbone when Ru-red is converted into Ru-brown [54]. Incomplete conversion of Ru-red into Ru-brown was found to produce smaller shifts [50,54]. However, in particular the frequency of the ν_1 Ru-O symmetric stretch involving the two oxygen adjacent to the central Ru ion is very sensitive to the Ru-red to Ru-

brown transition, which is thought to be related to the removal of an electron from an antibonding orbital located on the Ru-O-Ru-O-Ru backbone [54]. These spectral features allow the detection of the Ru-red to Ru-brown transition, which is one of the aims of our spectro-electrochemical experiment (Figs. 2.6, Table 1.1).

Table 1.1. Raman Shifts (wavenumbers cm^{-1}) for Ru-red in solution.

Compound		Raman Shifts (wavenumbers cm^{-1})*	
Ru-red	Ru-brown	Assignment	
157	178	ν_6	Ru-O
281	294	ν_5	O-Ru-N
376	390	$\nu_{2,3,4,8,9}$	Ru-N
396			
438	424		
486			
540			
744	778	ν_1	Ru-O
780			NH_3
825	840	ν_7	Ru-O

*in accordance with Ref. 49-51.

In Figure 2.6a, at low potential (0.64 V), the spectrum clearly indicates the presence of Ru-red near or on the electrode surface. The band at 156 cm^{-1} has been attributed to the ν_6 Ru-O stretching frequency; the same vibration in Ru-brown has been observed at 178 cm^{-1} [50], while it is not observed in the spectrum at 0.64 V. The feature at 280 cm^{-1} has been assigned to the O-Ru-N bending vibration, and it supposedly shifts to higher wavenumbers (*ca.* 294 cm^{-1}) for Ru-brown. The smaller features at 378, 421 and 510 cm^{-1} could correspond to Raman shifts observed for either Ru-red or Ru-brown, but the pair of features observed at 746 and 835 cm^{-1} appears as characteristics for Ru-red. Both modes are Ru-O

stretching modes, reported at 744 and 825 cm^{-1} for Ru-red in solution (the corresponding modes for Ru-brown are at 778 and 840 cm^{-1}). Considering the dominance of the modes at 156, 280, and 746 cm^{-1}, which are all characteristic of Ru-red (see also Table 1.1), we derive that the species most prominently observed at 0.64 V is Ru-red.

As the electrode potential is stepped positively, some important spectral changes are observed as shown in Figure 2.6. In general, changes in intensity and frequency may be related to three different effects: a change in identity of the species (*e.g.* a conversion from Ru-red to a Ru-brown type species) as a result of a change in electrode potential, a change in orientation or structure of the adsorbed Ru-red (or Ru-brown), or an electrochemical Stark tuning effect in which the electric field existing at the interface leads to changes in the vibrational frequencies and the intensity of the SERS lines of the adsorbed species [55]. As stated earlier, the SER spectra of Ru-red in Figure 2.6a show predominantly Ru-red features at the start of the positive potential scan (0.64 V). The band at 280 cm^{-1} shifted to a higher wavenumber *ca.* 295 cm^{-1} at 0.74 V (vs. NHE) indicating the possible formation of Ru-brown or similar species near the Au electrode at this potential, though the 156 and 745 cm^{-1} bands seem to be unaffected. However, the 156 cm^{-1} band decreases in intensity with the positive-rising potential. In spite of the continued dominance of the spectral pair at 740 and 835 cm^{-1} at higher potentials, which we ascribe to Ru-red, the disappearance of the band at 157 cm^{-1} and the shift of the band at 280 to 295 cm^{-1}, may indicate the formation of a (small) amount of Ru-brown or a similar species at potentials higher than ca. 0.7 V (vs. NHE).

In a previous report by the Kaneko group, the transition of Ru-red to Ru-brown has been observed by *in situ* electrochemical visible absorption spectral studies in a phosphate buffer solution at pH=7.4 on a thin layer ITO electrode during oxidative scans from 0.42 to 0.75V (vs. NHE) [32]. Although the SER spectra in Figure 2.6a contribute to converging evidence for the Ru-red conversion into the Ru-brown at this potential [28,32-34], some features attributable to Ru-red remain present even at this potential. The RRDE experiment revealed that water oxidation may occur at

low overpotential (Fig. 2.2) catalyzed by Ru-red, suggesting the formation of higher oxidation state Ru species like Ru^{V}-O-Ru^{V}-O-Ru^{V} or similar intermediates and their possible involvement in water oxidation process. Above this potential, gold oxide species (as indicated by a broad Raman band at 588 cm^{-1}) are observed similar to bare gold in the same electrolyte but without Ru-red in the solution (see Fig. A2.4).

Figure 2.6b shows the SER spectra obtained at selected potentials on the Ru-red functionalized Au electrode (RRA) without Ru-red in solution. Raman bands at 281, 745 and 829 cm^{-1} and a small broad band at *ca.* 159 cm^{-1} at low potential (0.64 V) suggesting the presence of (adsorbed) Ru-red on the Au_{disk} (Table 1.1). At 1.24 V (vs. NHE), the Raman bands at *ca.* 159 cm^{-1} and 745 cm^{-1} have shifted to *ca.* 174 cm^{-1} and 770 cm^{-1} respectively, providing evidence for formation of a Ru-brown type species at this potential. However, no profound changes were observed in the 281 cm^{-1} band. Compared to SER spectra on the gold electrode with Ru-red in the solution (Fig. 2.6a), the SERS analysis of RRA (without Ru-red in the electrolyte solution) shows a delayed appearance of the formation of Ru-brown signals (Fig. 2.6b) suggesting a different catalytic behaviour of Ru-red for the two systems deposited on the roughened gold electrode, in agreement with the different applied electrode potentials at which the two systems show catalytic characteristics for oxygen evolution (Fig. 2.2).

With more than 1.34 V applied to the RRA, additional Raman peaks are observed at *ca.* 529, 659, and 711 cm^{-1}. These modes may be associated with the formation of decomposition products in the catalyst [50]. Gold oxide vibrations can be discerned in the Raman spectra at potentials above 1.44 V. In order to compare the Ru-red features with the ruthenium oxide during water oxidation, a thin hydrous film of electrodeposited ruthenium oxide ($RuO_x \cdot nH_2O$) was also investigated by spectro-electrochemical Raman experiments. The SER spectra of a hydrous ruthenium oxide freshly electrodeposited on a roughened gold disk electrode were collected in a 0.1 M H_2SO_4 aqueous electrolyte without Ru-red or free Ru in the solution (Fig. A2.5).

Raman shifts observed at wavenumber 522, 665 and 742 cm^{-1} would be indicative of the presence of ruthenium oxide as it is found to be Raman active in the range of 450-800 cm^{-1} as vibrational modes [56,57]. The intensities of these bands gradually decrease by increasing the potential to more positive values, suggesting the conversion or loss of the ruthenium oxide species on the gold surface. The SER spectra show that the features ascribable to the electrodeposited ruthenium oxide ($RuO_x \cdot nH_2O$) on the Au_{disk} are present until 1.24 V, (Fig. A2.5), essentially just before the water oxidation sets in (as seen in the RRDE experiment in Fig. 2.3). For potentials above 1.24 V, the ruthenium oxide features disappear and a broad band at 597 cm^{-1} due to the formation of gold oxide on the surface dominates the spectrum (See also Fig. A2.4).

Summarizing, the Raman spectra of Ru-red on bare gold with Ru-red in solution, of the Ru-red functionalized gold electrode, and of Ru-oxide modified gold electrode, all show different and distinctive features. For the two systems with Ru-red, the Raman data suggest a transition from Ru-red to a Ru-brown type species with increasing potential, and the transition appears to take place at significantly more positive potentials when Ru-red is only on the surface and not in solution. The delay in oxidation behaviour is mirrored by the activity for water oxidation, which also occurs at significantly more positive potentials for the Ru-red functionalized gold electrode without Ru-red in solution. In particular for the latter system, Raman active modes are observed close to the onset of oxygen evolution. These modes show some resemblance to the Raman features observed for ruthenium oxide. Such features are not clearly observed for the system with Ru-red in solution, while the catalytic activity of the system is similar to that of the gold electrode modified with Ru-oxide.

2.3. CONCLUSIONS

In this chapter, catalytic oxidation of water by Ru-red in acidic media with successfully employing the electrochemical rotating ring-disk electrode (RRDE), online electrochemical mass spectrometry (OLEMS), and *in situ* surface enhanced Raman spectroscopy (SERS) for spectro-electrochemical investigations during water splitting catalysis, is discussed. Oxygen evolution and detection experiments using Ru-red and electrodeposited ruthenium oxide were conducted on RRDE, revealing oxygen evolution currents complemented by a corresponding reduction current at the platinum ring electrode. OLEMS measurements validate the RRDE findings for the Ru-red functionalized gold electrode that displays water oxidation just above 1.45 V (vs. NHE). In contrast, with deposition on a bare gold electrode in sulphuric acid solution containing Ru-red, the onset of oxygen evolution seems to start at ~1.23 V (vs. NHE) but not supported by the OLEMS analysis. SERS experiments show that Ru-red undergoes electro-induced oxidative conversion to a higher oxidation state ruthenium compound, probably a form of Ru-brown, at *ca*. 0.74 V (vs. NHE). The Ru-brown type species subsequently loses three more electrons and, ultimately, oxidizes water to make dioxygen [28-32]. In another set of experiments on the electrodeposited ruthenium oxide film on the Au_{disk}, the onset of oxygen evolution is observed at *ca*. 1.30 V (vs. NHE). Thus, electrochemical methods to test catalytic water oxidation using a commercially available trinuclear ruthenium complex are described here. The RRDE method is exploited to study oxygen evolution and detection experiments and results are validated with the OLEMS measurements.

2.4. MATERIALS AND METHODS

Potassium ferricyanide ($K_3[Fe(CN)_6]$), $RuCl_3.nH_2O$ and Ru-red ($[(NH_3)_5Ru\text{-}O\text{-}Ru(NH_3)_4\text{-}O\text{-}Ru(NH_3)_5]Cl_6$) were of reagent grade, obtained from Sigma-Aldrich Co., and used as received. All the solutions were prepared in ultra-pure water (Millipore MilliQ® A10 gradient, 18.2 MΩ cm, 2–4 ppb total organic content). All

solutions were purged with high-purity argon (Linde Gas, 6.0) for at least 30 min before each measurement to minimize the oxygen interference during electrochemical investigations. An argon atmosphere was maintained both in and above the solution during the electrochemical measurements to make sure that no air/oxygen was entering and intervening with the electrochemical system.

All glassware and cells were cleaned by boiling in a 1:1 mixture of concentrated nitric acid and sulfuric acid (for 2 hours and left overnight). Next, the glassware was washed and boiled in ultra-pure water and dried in an oven at 65° C. The cell was boiled and washed thoroughly with ultra-pure water before each experiment. All the electrochemical work was conducted in a conventional single-compartment three-electrode glass cell and RRDE experiments were performed in a home-made RRDE glass cell. A three electrode configuration spectro-electrochemical glass cell, having an optical quartz window at the bottom parallel to the gold working electrode, was employed for the electrochemical SERS investigation.

A polycrystalline gold and basal plane graphite disks (diameter d=5mm) were used as working electrode (WE) in voltammetry. A platinum disk (diameter d=5mm) was employed in the collection efficiency experiment. The working electrode in the SERS experiments was a roughened polycrystalline gold disk (diameter d=5mm) embedded in a PTFE shroud. A platinum wire (thickness: 1 mm), was used as a counter electrode (CE) and the reference electrode (RE) was a mercury–mercury sulfate electrode (MMSE: $Hg/Hg_2SO_4/K_2SO_4$). However, all potentials are referred to the normal hydrogen electrode (NHE). Rotating ring-disk electrode measurements were carried out on the RRDE-system with an AFMSRX rotator and a MSRX speed controller (Pine Instrument Company, Grove City, PA, USA). For oxygen detection measurements, the RRDE setup consisted of a mirror finished polished polycrystalline Au_{disk} (radius $r_1 = 0.250$ cm, area $A_{disk}=0.196$ cm^2) and a concentric Pt_{ring} (inner radius $r_2 = 0.325$ cm; outer radius $r_3 = 0.375$ cm; area $A_{ring}=0.11$ cm^2). The theoretical collection efficiency, N = 25.6%, was confirmed by standard experiments with the ferri-/ferro-cyanide couple [43].

Figure 2.7. Set up for RRDE assembly showing (**a**) working electrode (WE) disks, (**b**) ring and tip and (**c**) the rotor with a speed controller (taken from Pine Inst. web).

An EvoLution mass spectrometer system (European Spectrometry Systems Ltd.) was employed for on-line electrochemical mass spectrometry measurements. The pressure inside the mass spectrometer (MS) was 1×10^{-6} – 5×10^{-6} mbar during OLEMS measurements. Further details of the experimental parameters, pretreatment procedures and instrument operation are described previously [58]. SERS analysis was performed with a HR 800 spectrograph (Jobin Yvon) with a holographic grating of 600 gr mm^{-1}. The confocal hole of the instrument was set at 100 μm. A CCD camera with 1024 × 256 pixels was used as detector. The excitation line source was provided by a 20 mW HeNe laser at 632.8 nm. The laser beam was focused through an Olympus 50× microscope objective, which was not immersed in the electrolyte, into a 5 μm spot on the electrode surface. A notch filter was used to filter the SERS signal before reaching the sample. With this configuration, a resolution of 1.2 cm^{-1} was obtained [59]. Surface enhancement of the gold disk by roughening the gold surface was done by applying 25 potential sweep oxidation-reduction cycles consecutively in 0.1 M KCl (Merck, pro analysis) from 1.25 to –0.25 V versus the saturated calomel electrode (SCE: $Hg/Hg_2Cl_2/KCl$) [60].

Cyclic voltammetry, forward potential scans and other electrochemical investigations for RRDE measurements, OLEMS analyses and *in situ* SERS investigations were performed with a computer-controlled IviumStat (Ivium

Technologies, Eindhoven, The Netherlands) and operated by IviumSoft. Prior to the actual experiments, Au_{disk} and Pt_{ring} were polished mechanically with an aqueous slurry of 0.3, 0.1 and 0.05 μm alumina (Buehler Limited) successively, on a Microcloth polishing fabric, until a mirror finish was achieved. After polishing, the electrodes were ultrasonically cleaned in Milli-Q (Millipore) water for 15–20 minutes after each polishing step and rinsed thoroughly with pure water. A spiral platinum counter electrode was flame annealed and washed with pure water before placing into the cell.

Pure argon gas was purged into the 0.1 M H_2SO_4 electrolyte solution for at least 30 minutes at a rotation rate of 1200 rpm before the oxygen evolution-detection experiment with the Au_{disk}-Pt_{ring} RRDE assembly. This step is very important in order to ensure the complete removal of oxygen from the test solution which can possibly interfere with the oxygen detection/reduction measurements. Oxygen elimination from the continuously Ar-bubbled 0.1 M H_2SO_4 aqueous solution was carefully verified by scanning the freshly polished Pt_{ring} electrode on the RRDE assembly between +1.44 V and +0.02 V (vs. NHE) from 500-2500 rpm until no oxygen reduction/detection current was observed. After this confirmation, the Au_{disk} was fitted to the RRDE for oxygen evolution studies in Ar-saturated 0.1M H_2SO_4 aqueous solution. It was then cyclized between 0.64–2.04 V (vs. NHE) and the Pt_{ring} was potentiostated at +0.44 V (vs. NHE) at a rotation rate of 700 rpm.

Prior to the water splitting and oxygen measurements experiments, the Au_{disk} and Pt_{ring} were electrochemically pre-treated in 0.1 M $HClO_4$ or 0.05 M H_2SO_4 by scanning the potential between 0.5–2.1 V and +1.7 to –0.2 V (vs. NHE) respectively, for 50 cycles at 50 mV/sec. This procedure provided good reproducibility of the data [61]. After potential cycling, the electrodes were immediately transferred to another cell containing O_2-deaerated Ar-saturated 0.1 M aqueous sulphuric acid solution in order to avoid surface contamination in air. For oxygen detection/reduction experiments in 0.1 M aqueous sulphuric acid solution,

the potential of the Pt_{ring} was held at +1.44 V (vs. NHE) for 5 seconds and scanned between +1.44 and +0.02 V (vs. NHE) at 20 mV/sse.

Two types of experiments were conducted for oxygen evolution from water splitting by the Ru-red catalyst. In the first type of experiment, an aliquot of Ru-red catalyst solution, prepared in a small quantity of O_2-deaerated deionized water, was dissolved in O_2-deaerated Ar-saturated aqueous 0.1 M H_2SO_4 solution before the catalytic water oxidation experiment. The resulting Ru-red concentration was 0.035 mM. In the second type of experiment, Ru-red was immobilized on the Au_{disk} by adsorption. Ru-red does not bind strongly to a mirror-finish Au surface, and therefore, a roughened gold surface was prepared to which Ru-red binds more strongly. The catalyst was immobilized by placing 15 μL of a stock solution of Ru-red (0.05 mM), prepared in ultrapure deoxygenated water, on the roughened Au surface. It was dried for 4–6 hours and the same procedure was repeated 5 times. The electrode was subsequently left for at least 32–34 hours. After this procedure, it was rinsed with ultrapure water to remove the unattached Ru-red molecules and employed directly for electrochemical investigation without any delay.

A thin hydrous ruthenium oxide ($RuO_x \cdot nH_2O$) film was electrochemically deposited on a freshly roughened Au_{disk} from 0.01 M HCl and 0.1 M potassium chloride electrolytes containing 1 mM $RuCl_3$ in a deoxygenated aqueous solution (pH ≈ 2) by a procedure described in the literature [62]. In our experimental setup, the electrodeposition of the $RuO_x \cdot nH_2O$ film was realized by scanning the potential of the Au_{disk} electrode from 0.10–1.04 V (vs. NHE) for 160–180 cycles in the above chloride electrolyte solution at a scan rate of 50 mV/sec. The ruthenium oxide film thus produced was washed with pure water and employed without any further treatment in SERS and anodic water oxidation experiments using the RRDE setup.

REFERENCES

01- T. N. Verziroglu and F. Barbir, *Int. J. Hydrogen Energy* **1992**, *17*, 391–404.

02- J. E. Funk, *Int. J. Hydrogen Energy* **2001**, *26*, 185–190.

03- C. A. Grimes, O. K. Varghese and S. Ranjan, *Light, Water, Hydrogen: The Solar Generation of Hydrogen by Water Photoelectrolysis*, Springer Science + Business Media: New York, **2008**; Ch. 2.

04- A. J. Bard, *J. Am. Chem. Soc.* **2008**, *130*, 8565–8568.

05- T. J. Meyer, *Nature* **2008**, *451*, 778–779.

06- N. S. Lewis, *Nature* **2001,** *414*, 589–590.

07- X. Sala, M. Rodriguez, I. Romero, L. Escriche and A. Llobet, *Angew. Chem., Int. Ed.* **2009**, *48*, 2842–2852.

08- K. N. Ferreira, T. M. Iverson, K. Maghlaoui, J. Barber and S. Iwata, *Science* **2004**, *303***,** 1831–1838.

09- J. Yano, J. Kern, K. Sauer, M. J. Latimer, Y. Pushkar, J. Biesiadka, B. Loll, W. Saenger, J. Messinger, A. Zouni and V. K. Yachandra, *Science* **2006**, *314*, 821–825.

10- J. P. McEvoy and G. W. Brudvig, *Chem. Rev.* **2006,** *106*, 4455–4483.

11- A. W. Rutherford and A. Boussac, *Science* **2004**, *303*, 1782–1784.

12- M. Haumann, P. Liebisch, C. Müller, M. Barra, M. Grabolle and H. Dau, *Science* **2005**, *310*, 1019–1021.

13- L. Hammarström and S. Styring, *Phil. Trans. R. Soc. B* **2008**, *363*, 1283–1291.

14- J. A. Gilbert, D. S. Eggleston, W. R. Murphy, *Jr.* D. A. Geselovitz, S. W. Gersten, D. J. Hodgson and T. J. Meyer, *J. Am. Chem. Soc.* **1985**, *107*, 3855–3864.

15- T. Wada, K. Tsuge and K. Tanaka, *Angew. Chem., Int. Ed. Engl.* **2000**, *39*, 1479–1482.

16- C. Sens, I. Romero, M. Rodrıguez, A. Llobet, T. Parella and J. Benet-Buchholz, *J. Am. Chem. Soc.* **2004**, *126*, 7798–7799.

17- J. K. Hurst, *Coord. Chem. Rev.* **2005**, *249*, 313–328.

18- R. Zong and R. P. Thummel, *J. Am. Chem. Soc.* **2005**, *127*, 12802–12803.

19- P. Kurz, G. Berggren, M. F. Anderlund and S. Styring, *J. Chem. Soc. Dalton Trans.* **2007**, 4258–4261.

20- M. W. Kanan and D. G. Nocera, *Science* **2008,** *321*, 1072–1075.

21- J. Limburg, J.S. Vrettos, L.M. Liable-Sands, A.L. Rheingold, R.H. Crabtree and G.W. Brudvig, *Science* **1999**, *283*, 1524–1527.

22- Z. Deng, H.-W. Tseng, R. Zong and R. Thummel, *Inorg. Chem.* **2008**, *47*, 1835-1848.

23- F. Liu, T. Cardolaccia, B. J. Hornstein, J. R. Schoonover and T. J. Meyer, *J. Am. Chem. Soc.* **2007**, *129*, 2446–2447.

24- W. F. Ruettinger, C. Campana and G. C. Dismukes, *J. Am. Chem. Soc.* **1997,** *119,* 6670–6671.

25- J. Mola, E. Mas-Marza, X. Sala, I. Romero, M. Rodriguez, C. Viñas, T. Parella and A. Llobet, *Angew. Chem. Int. Ed.* **2008**, *47*, 5830–5832.

26- J. T. Muckerman, D. E. Polyansky, T. Wada, K. Tanaka and E. Fujita, E. *Inorg. Chem.* **2008**, *47*, 1787–1802.

27- C.W. Cady,R. H. Crabtree and G. W. Brudvig, *Coord. Chem. Rev.* **2008**, *252*, 444–455.

28- R. Rarnaraj, A. Kira and M. Kaneko, *Angew. Chem. Int. Ed. Engl.* **1986,** *25*, 1009–1011.

29- S.Yamashita, K. Nagoshi, M. Yagi amd M. Kaneko, *J. Mol. Catal. A* **2000**, *153*, 209–214.

30- M. Yagi, E. Takano and M. Kaneko, *Electrochim. Acta* **1999**, *44*, 2493–2497.

31- M. Yagi, K. Kinoshita and M. Kaneko, *Electrochim. Acta* **1999**, *44*, 2245–2250.

32- R. Rarnaraj and M. Kaneko, *J. Mol. Catal.* **1993**, *81*, 319–332.

33- G. J. Yao, A. Kira and M. Kaneko, *J. Chem. Soc. Faraday Trans.1* **1988**, *84*, 4451–4456.

34- R. Ramaraj, A. Kira and M. Kaneko, *J. Chem. Soc. Faraday Trans.1* **1987**, *83,* 1539–1551.

35- D. E. Burchfield and R. M. Richman, *Inorg. Chem.* **1985**, *24,* 852–857.

36- S. Trasatti, *Electrochim. Acta* **1984,** *29*, 1503–1512.

37- M. Yagi, Y. Takahashi, I. Ogino and M. Kaneko, *J. Chem. Soc., Faraday Trans.* **1997**, *93*, 3125–3127.

38- M. Yagi, I. Ogino, A. Miura, Y. Kurimura and M. Kaneko, *Chem. Lett.* **1995**, *24*, 863.

39- I. Ogino, K. Nagoshi, M. Yagi and M. Kaneko, *J. Chem. Soc., Faraday Trans.* **1996**, *92*, 3431–3434.

40- J. Haenen, W. Visscher and E. Barendrecht, *J. Electroanal. Chem.* **1986**, *208*, 273–296.

41- M. Vuković, *J. Chem. Soc. Faraday Trans.* **1990**, *86*, 3743–3748.

42- Y. Hu, Y. V. Tolmachev and D. A. Scherson, *J. Electroanal. Chem.* **1999**, *468*, 64–69.

43- (a) S. Han, J. Zhai, L. Shi, X. Liu, W. Niu, H. Li and G. Xu, *Electrochem. Commun.* **2007**, *9*, 1434–1438. (b) M.-G. Vergé, P. Mettraux, C.-O.A. Olsson and D. Landolt, *J. Electroanal. Chem.* **2004**, *566*, 361–370.

44- U. A. Paulus, T. J. Schmidt, H. A. Gasteiger and R. J. Behm, *J. Electroanal. Chem.* **2001**, *495*, 134–145.

45- P. R. Birkin, J. M. Elliott and Y. E. Watson, *Chem. Commun.* **2000**, 1693–1694.

46- R. Kötz, S. Stucki, D. Scherson and D. M. Kolb, *J. Electroanal. Chem.* **1984**, *172*, 211–219.

47- M. Wohlfahrt-Mehrens and J. Heitbaum, *J. Electroanal. Chem.* **1987**, *237*, 251–260.

48- H. Ma, C. Liu, J. Liao, Y. Su, X. Xue and W. Xing, *J. Mol. Catal. A: Chemical* **2006**, *247*, 7–13.

49- J. M. Friedman, D. L. Rousseau, G. Navon, S. Rosenfeld, P. Glynn and K. B. Lyons, *Arch. Biochem. Biophys.* **1979**, *193*, 14–21.

50- M. Itabashi, K. Shoji and K. Itoh, *Chem. Lett.* **1981**, *10*, 491–494.

51- M.A.A.F. de C.T. Carrondo, W.P. Griffith, J.P. Hall and A.C. Skapski, *Biochimica et Biophysica Acta* **1980**, *627*, 332–334.

52- J. M. Fletcher, B. F. Greenfield, C. J. Hardy, D. Scargill and J. L. Woohead, *J. Chem. Soc. (Lond.)* **1961**, 2000–2006.

53- J. E. Earley and T. Fealey, *Inorg. Chem.* **1973**, *12*, 323–327.

54- J. R. Campbell, R. J. H. Clark, W. P. Griffith and J. P. Hall, *J. Chem. Soc., Dalton Trans.***1980**, 2228–2236.

55- S. A. Wasileski, M. T. M. Koper and M. J. Weaver, *J. Chem. Phys.* **2001**, *115*, 8193-8203.

56- S. Bhaskar, P. S. Dobal, S. B. Majumder and R. S. Katiyara, *J. Appl. Phys.* **2001**, *89*, 2987–2992.

57- S. Y. Mar, C. S. Chen, Y. S. Huang and K. K. Tiong, *Appl. Surf.Sci.* **1995**, *90*, 497–504.

58- (a) A. H. Wonders, T. H. M. Housmans, V. Rosca and M. T. M. Koper, *J. Appl. Electrochem.* **2006**, *36*, 1215-1221. (b) M. Duca, M. O. Cucarella, P. Rodriguez and M. T. M. Koper, *J. Am. Chem. Soc.* **2010**, *132*, 18042–18044.

59- (a) S. C. S. Lai, S. E. F. Kleyn, V. Rosca and M. T. M. Koper, *J. Phys. Chem. C*, **2008**, *112*, 19080–19087. (b) P. Corio and J. C. Rubim, *J. Raman Spectrosc.* **1997**, *28*, 235–241.

60- P. Gao, D. Gosztola, L. W. H. Leung and M. J. Weaver, *J. Electroanal. Chem.* **1987**, *233*, 211–222.

61- A. Sarapuu, A. Kasikov, T. Laaksonen, K. Kontturi and K. Tammeveski, *Electrochim. Acta* **2008**, *53*, 5873–5880.

62- C.-C. Hu and Y.-H. Huang, *Electrochim. Acta* **2001**, *46*, 3431–3444.

Appendix A2

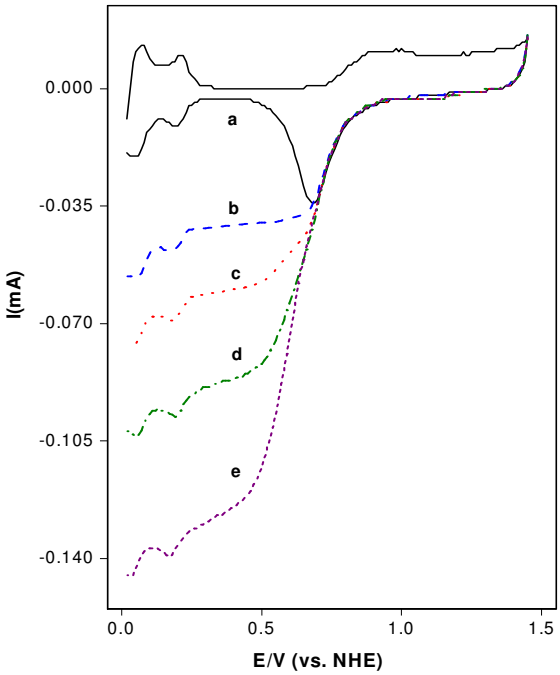

Figure A2.1.
Current potential curves for oxygen reduction on the Pt ring at Au_{disk} potentials (a) 0.0 V, (b) 1.75 V, (c) 1.85 V, (d) 1.95 V and (e) 2.05 V in deoxygenated Ar-saturated 0.1 M H_2SO_4 solution at 700 rpm, scan rate 20 mV/sec, E/V vs. NHE. Pt_{ring} was potentiostated at 0.44 V (vs. NHE).

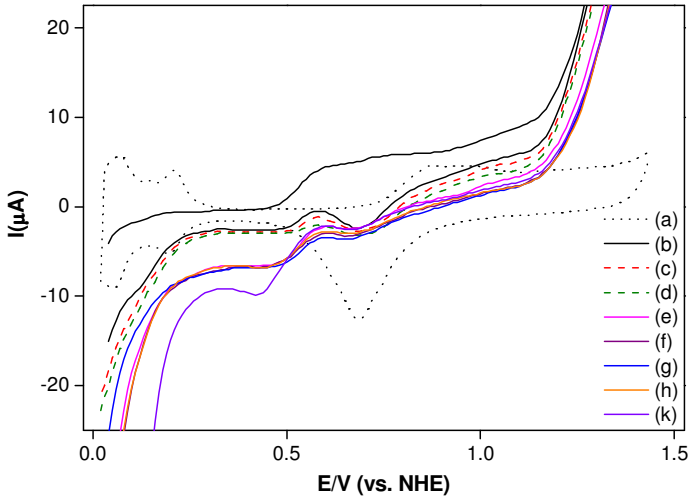

Figure A2.2. Current potential curves for oxygen reduction on the Pt ring in deoxygenated 0.1 M H_2SO_4 solution without Ru-red at Au_{disk} potentials (a) 0.0 V and in deoxygenated 0.1 M H_2SO_4 solution containing 0.035 mM Ru-red at (b) 0.0 V, (c) 1.21 V, (d) 1.22 V, (e) 1.23 V, (f)1.25 V, (g) 1.30 V (h) 1.40 V and (k) 1.50 V. Oxygen is generated by catalytic water oxidation in the presence of Ru-red in the aqueous electrolyte solution. Rotation rates were 700 rpm, scan rates 20 mV/sec and the ring potential was 0.44 V (vs. NHE).

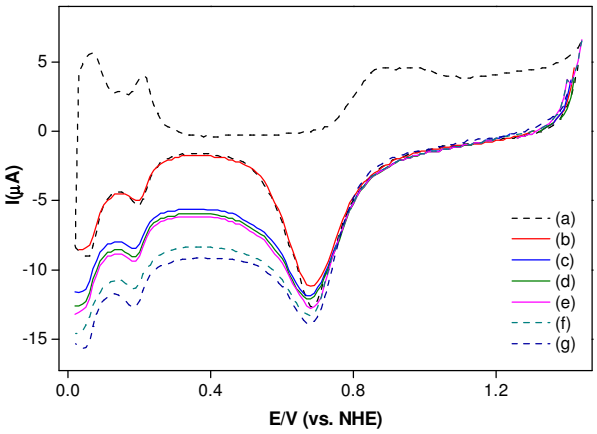

Figure A2.3.
Current potential curves for oxygen reduction on the Pt ring at Au_{disk} [functionalized with Ru-red (RRA)] potentials (a) 0.0 V, (b) 1.43 V, (c) 1.44 V, (d) 1.45 V, (e) 1.50 V, (f) 1.75 V and (g) 1.85 V in deoxygenated 0.1 M H_2SO_4 electrolyte solution. Oxygen is generated by catalytic water oxidation on the RRA. Rotation rates were 700 rpm, scan rates 20 mV/sec and the ring potential was 0.44 V (vs. NHE).

Figure A2.4.

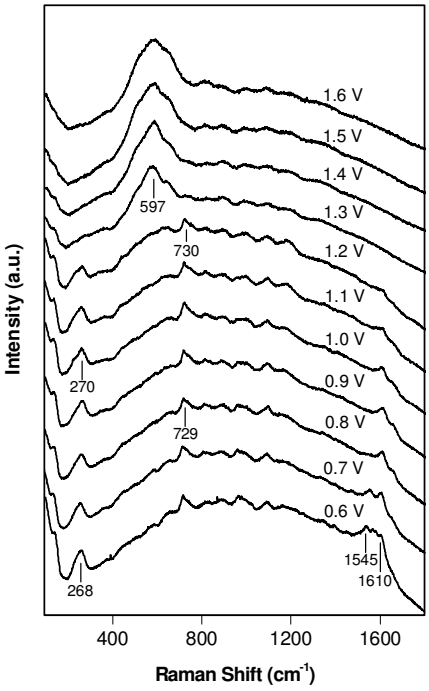

Figure A2.5.

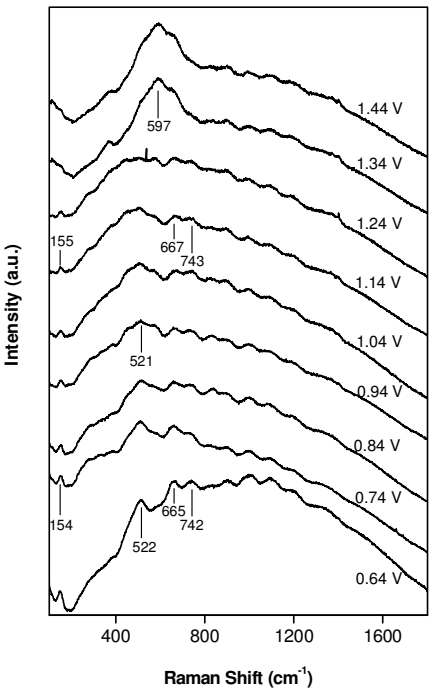

Figure A2.4. *In situ* electrochemical SERS spectra of a freshly polished and roughened Au_{disk} electrode at selected potentials in deoxygenated Ar-saturated 0.1 M H_2SO_4 aqueous electrolyte without Ru-red in solution. The starting potential was 0.6 V and was successively incremented up to 1.6 V (vs. NHE).

Figure A2.5. Selected potential-dependent *in situ* electrochemical SER spectra for a hydrous ruthenium oxide ($RuO_x \cdot nH_2O$) film that was freshly electrodeposited on a roughened Au_{disk} electrode and scanned in the deoxygenated and Ar-saturated 0.1 M H_2SO_4 electrolyte solution. The starting potential was 0.6 V and was successively incremented up to 1.4 V (vs. NHE).